University of Groningen

Label-Free and Real-Time Detection of Protein Ubiquitination with a Biological Nanopore

Wloka, Carsten; Van Meervelt, Veerle; van Gelder, Dewi; Danda, Natasha; Jager, Nienke; Williams, Chris P; Maglia, Giovanni

IMPORTANT NOTE: You are advised to consult the publisher's version (publisher's PDF) if you wish to cite from it. Please check the document version below.

Document Version
Publisher's PDF, also known as Version of record

[Link to publication in University of Groningen/UMCG research database](#)

ACS NANO

ARTICLE

Label-Free and Real-Time Detection of Protein Ubiquitination with a Biological Nanopore

Carsten Wloka,[†] Veerle Van Meervelt,[‡] Dewi van Gelder,[§] Natasha Danda,[§] Nienke Jager,[†] Chris P. Williams,*,[§] and Giovanni Maglia*,[†]

[†]Chemical Biology I, Groningen Biomolecular Sciences and Biotechnology Institute (GBB), University of Groningen, 9747 AG Groningen, The Netherlands

[‡]Department of Chemistry, University of Leuven, 3001 Leuven, Belgium

[§]Molecular Cell Biology, Groningen Biomolecular Sciences and Biotechnology Institute (GBB), University of Groningen, 9747 AG Groningen, The Netherlands

S *Supporting Information*

ABSTRACT: The covalent addition of ubiquitin to target proteins is a key post-translational modification that is linked to a myriad of biological processes. Here, we report a fast, single-molecule, and label-free method to probe the ubiquitination of proteins employing an engineered Cytolysin A (ClyA) nanopore. We show that ionic currents can be used to recognize mono- and polyubiquitinated forms of native proteins under physiological conditions. Using defined conjugates, we also show that isomeric monoubiquitinated proteins can be discriminated. The nanopore approach allows following the ubiquitination reaction in real time, which will accelerate the understanding of fundamental mechanisms linked to protein ubiquitination.

KEYWORDS: *nanotechnology, nanopore, single-molecule kinetics, protein modifications, ubiquitin*
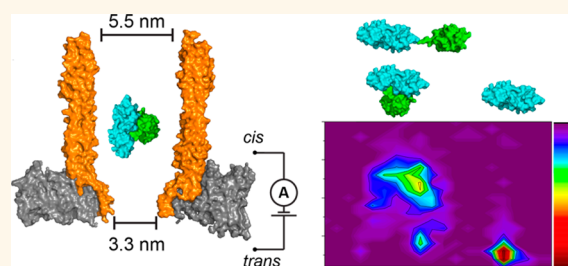
Post-translational modifications (PTMs) regulate the function of a vast range of proteins in a eukaryotic cell. The attachment of the small 8.6 kDa protein ubiquitin (Ub) to a substrate protein (ubiquitination) can affect its fate in many ways, from signaling its degradation to altering its cellular location or inhibiting its interaction with other proteins. Ubiquitination is achieved through the activity of three different enzymes.[1,2] First, an ubiquitin activating enzyme (E1) activates Ub through the hydrolysis of ATP. Next, the E1 transfers Ub to the active site cysteine of a ubiquitin-conjugating enzyme (E2), which, with the aid of an E3 ligase, attaches Ub to a substrate protein, often to a lysine residue (Figure 1A).

Abnormal concentration of ubiquitin and/or the precise ubiquitination of protein substrates are linked to disease. For example, ubiquitin levels have been observed to increase in cerebrospinal fluid of patients with Alzheimer's disease,[3] while ubiquitinated substrates, including E2 enzymes, are directly implicated in human disease.[4] Further, aberrant ubiquitination of α-synuclein, a protein involved in Parkinson's disease, may affect aggregation depending on which lysine residue is modified.[5] It follows that the detection of the exact pattern and position of ubiquitination of a protein substrate is a potentially useful biomarker for disease onset and progression.[6,7]

Currently, only ensemble methods that use either fluorescently labeled ubiquitin[8] or substrates[9] allow real-time monitoring of the ubiquitination reaction *in vitro*. Such methods, however, do not allow monitoring the entire ubiquitination cascade of E1−E2−E3 or the simultaneous modification of multiple substrates. Further, since ubiquitination relies on precise interactions between proteins, fluorescent substrates often alter the kinetics and efficiency of the ubiquitination reaction.[10] Therefore, single-molecule and label-free methods can enhance our understanding of the factors that regulate ubiquitination.

Biological nanopores are powerful tools to study single molecules. In nanopore analysis, the signal is provided by the ionic current generated by hydrated ions translocating through the nanopore under an external applied potential. Molecules entering the nanopore by either passive diffusion or sustained by the electrical potential or the electro-osmotic flow are recognized by the specific modulation of the nanopore current. Nanopores have been used to sense molecules[11−14] and to monitor chemical and enzymatic reactions[15−18] to study nucleic acids[19−22] and folded proteins.[23−27] Unfolded proteins might
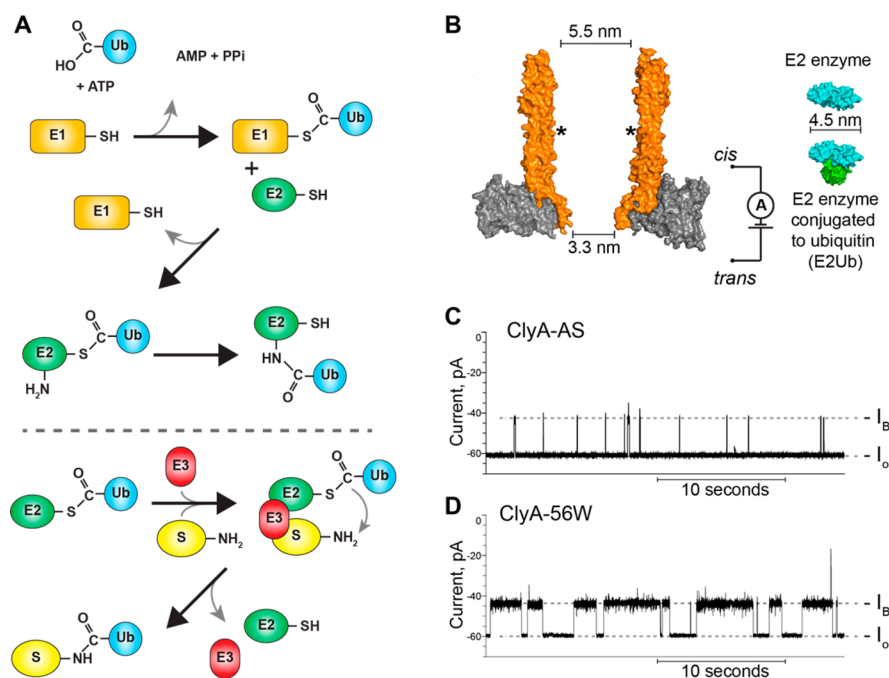
Figure 1. (A) Scheme of the ubiquitin cascade. Ubiquitin activating enzyme (E1) activates Ub through hydrolysis of ATP. Next, the E1 transfers Ub to the active site cysteine of a ubiquitin-conjugating enzyme (E2). E2 can transfer Ub further to one of its lysine residues or, with the help of a ubiquitin ligase (E3), ubiquitinate substrates (S). The part of the cascade above the dashed line we exploited to create E2 and its ubiquitinated form. (B) Left: ClyA nanopore (orange) from *Salmonella typhi*[47] lodged inside a lipid bilayer (gray) composed of 1,2-dioleoyl-*sn*-glycero-3-phosphocholine. Asterisks mark the approximate position of the glutamine to tryptophan substitution (Q56W). On the right are surface representations of the E2 Ub-conjugating enzyme Ubc4 (E2, cyan, PDB: 1QCQ) of *Saccharomyces cerevisiae* shown with and without Ub (green, PDB: 3CMM). The E2Ub conjugate models were constructed with PyMOL. The larger opening of ClyA is facing the *cis* compartment, whereas *trans* denotes the location of the "working" electrode. (C) Representative trace obtained with ClyA-AS after addition of the E2 enzyme (50 nM) added to the *cis* side of the nanopore. (D) E2 (50 nM) blockades elicited to ClyA-56W. I_O denotes the unobstructed open pore current; I_B is the blocked pore current as E2 dwells inside ClyA. Data in (C) and (D) were collected in 150 mM NaCl, 50 mM TrisHCl, pH 7.5 at −35 mV potential applied to the *trans* electrode and recorded using a 2 kHz low-pass Bessel filter with a 10 kHz sampling rate. Traces were postacquisition digitally filtered with a Gaussian 500 Hz low-pass filter.

also be studied as they translocate through nanopores with 1−2 nm of diameter.[27−32]

The identification of large PTMs such as ubiquitination may be achievable directly with nanopores. Using an immobilized DNA-conjugated model protein Bayley and co-workers showed that phosphorylation, another PTM, can be identified at different sites in unfolded polypeptides threading the nanopore.[33] However, at the moment, the unassisted translocation of polypeptides is too fast to allow the sequence identification of individual amino acids on the fly. Recently, Meller and co-workers demonstrated the detection and discrimination of single ubiquitin as well as short ubiquitin polymers with solid-state nanopores,[34] which may be useful to study length and linkage-type of ubiquitin chains once removed from a protein of interest. We have shown that folded proteins can be studied with the biological nanopore Cytolysin A (ClyA).[13] Because the 5.5 nm *cis* opening of ClyA is larger than its *trans* opening (3.3 nm, Figure 1B), proteins can remain trapped inside the nanopore for extensive time (*i.e.*, from milliseconds to hours depending on the size, charge, and shape of the protein)[13] and consequently recognized by the specific modulation of the nanopore current. In this work, we investigated the ability of nanopores to detect mono- and polyubiquitinated proteins. Using an engineered ClyA nanopore, we show that nanopore currents can be used to discriminate a protein from its mono- and polyubiquitinated derivatives and to discriminate defined isomeric monoubiquitinated proteins. Notably, all recordings

employed physiological conditions (Tris-buffered saline buffer: 150 mM NaCl, 50 mM TrisHCl, pH 7.5), sampled native proteins and allowed determining kinetic parameters of the E1 enzyme by observing the formation of the ubiquitinated E2 protein in real time. Collectively, our data put biological nanopores forward as a single-molecule tool for the detection and analysis of protein ubiquitination *in vitro*.

RESULTS AND DISCUSSION

Detection of Mono- and Poly-Ub Conjugates with an Engineered Biological Nanopore. To investigate whether ClyA can discriminate between a protein and its ubiquitinated form(s), we chose the ubiquitin-conjugating enzyme Ubc4 from the yeast *Saccharomyces cerevisiae* as a model protein. We relied on the fact that this E2 can ubiquitinate itself *in vitro*.[35] Many E2 enzymes are able to self-ubiquitinate, which might act as a regulator of E2 activity.[36] We employed this behavior to produce ubiquitinated protein in large amounts. In addition, we reasoned that the molecular weight of Ubc4 (19.8 kDa) and its ubiquitinated derivatives (+8.6 kDa) would be suitable for detection with ClyA nanopores (Figure 1B). We first added recombinantly expressed and purified Ubc4 (hereafter E2) (Figure S1A) to the *cis* side of a type I ClyA-AS[37] nanopore (C87A/L99Q/E103G/F166Y/I203V/C285S/K294R/H307Y), in a buffer containing 500 μL of 150 mM NaCl, 50 mM TrisHCl, pH 7.5, and applied a transmembrane potential of −35 mV (referring to the *trans* or "working electrode"). The

same buffer and applied potential were used throughout this study. We observed blockades (Figure 1C) with a residual current ($I_{res\%}$), defined as the ratio of amplitude percent of blocked pore (I_B) and open pore (I_O), of 72.9 ± 4.5%, with an average dwell time (or τ_{off}) of 39 ± 24 ms (mean ± SD; the mean and SD are obtained from N = 3 independent nanopore experiments, (Supporting Information Table 1). To prolong dwell times and thus potential resolution of isomeric ubiquitinated substrates, we used an engineered ClyA-AS nanopore where a tryptophan substituted a glutamine at position 56 (ClyA-Q56W, manuscript in preparation). Hence, an increased hydrophobic inner surface is created inside the lumen of ClyA-56W that would allow hydrophobic and electrostatic π interaction of proteins with the nanopore. Addition of 50 nM E2 to the *cis* side of ClyA-56W (henceforth ClyA, Figure 1D and Figure S1B) increased dwell times to 1737 ± 420 ms with similar $I_{res\%}$ of 74.0 ± 0.8% (N = 3), suggesting that E2 interacts with the inner surface of ClyA near position 56. The average capture rate (k_c), the inverse of the interevent time normalized for 1 μM of analyte, was 21.7 ± 3.6 s^{-1} μM^{-1}.

In order to obtain E2Ub conjugates, we performed *in vitro* ubiquitination reactions. As a negative control, we performed reactions in the absence of ATP. In those reactions, no ubiquitinated E2 was produced, as determined by SDS-PAGE and Coomassie staining (Figure 2). Addition of 5 μL of such a
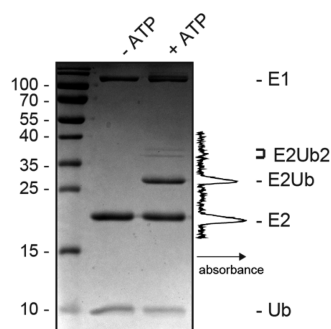

Figure 2. Coomassie-stained 15% SDS-PAGE gel of an E2 ubiquitination reaction with and without ATP. Protein marker (kDa) is shown on the left; the middle lane shows a ubiquitination reaction lacking ATP and on the right is a ubiquitination reaction shown with 5 mM ATP present. Both reactions were incubated for 2.5 h at 35 °C with shaking in buffer containing 75 mM NaCl, 25 mM TrisHCl, pH 8, 5 mM MgCl$_2$, recombinant Ub (12 μM), activating enzyme (E1, 0.4 μM), and E2 (6 μM). Depicted on the right of the gel is the intensity profile of the *in vitro* reaction ranging from beneath E2 to above E2Ub$_2$ with arbitrary absorbance units as determined with ImageJ (NIH).

reaction mixture containing no ATP to the 500 μL *cis* compartment of nanopores resulted in the formation of a single type of blockade, similar to the E2 alone, with $I_{res\%}$ 75.4 ± 0.3% (N = 3, τ_{off} = 2231 ± 481 ms, k_c = 6.6 ± 0.7 s^{-1} μM^{-1} (Figure 3A); thus the E1 and Ub do not produce blockades under these experimental conditions with ClyA. Consistently, we did not observe blockades when adding E1 and Ub in the absence of E2 (Figure S2). Therefore, E1 (molecular weight = 110 kDa) most likely is too large to enter the nanopore, whereas Ub (molecular weight = 8.6 kDa) molecules translocate too rapidly through ClyA. In support of this, we previously observed only very short transient events for lysozymes (molecular weight = 15 kDa).[13]
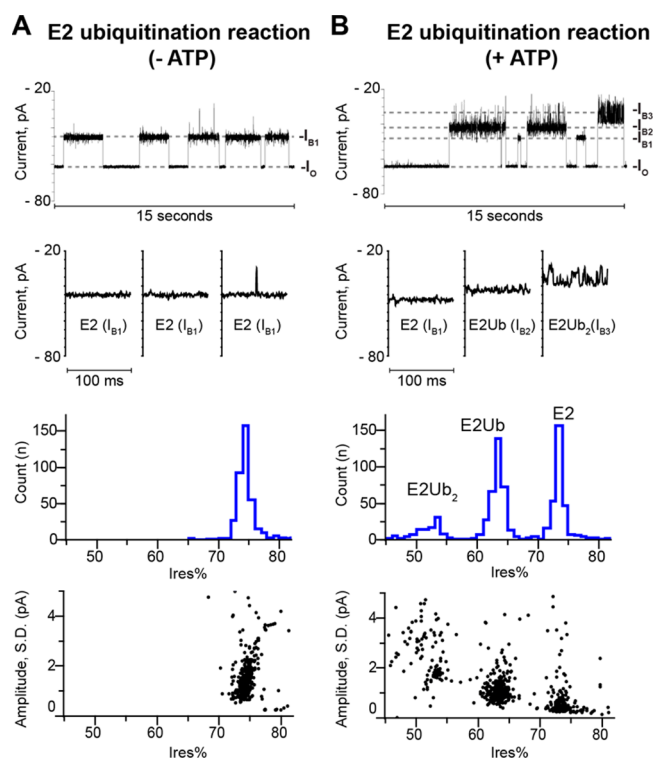

Figure 3. Detection of protein ubiquitination with ClyA nanopores. (A) From top to bottom: Representative trace (I_O = open pore and I_{B1} = blockade level, both at −35 mV), zoom-ins, histogram, and residual current percent ($I_{res\%}$) *versus* the standard deviation (SD) of individual current blockades elicited by E2 proteins. The blockades appeared after adding a 1:100 dilution (final) of the *in vitro* ubiquitination reaction described in Figure 2 (not containing ATP) to the *cis* side of the nanopore. (B) Same as in (A), but the ubiquitination reaction contained ATP. Note that Ub and E1 do not elicit blockades (Figure S1). Buffer used in all electrophysiological experiments: 150 mM NaCl, 50 mM TrisHCl, pH 7.5. Data were collected at −35 mV and recorded using a 2 kHz low-pass Bessel filter with a 10 kHz sampling rate. Traces were postacquisition digitally filtered with a Gaussian 500 Hz low-pass filter.

When ATP was present in *in vitro* ubiquitination reactions, efficient E2 self-ubiquitination was occurring, as determined by SDS-PAGE and Coomassie staining (Figure 2). The major product of the reaction was monoubiquitinated E2, but a small amount of E2 carrying two Ubs was also produced, in line with our previous data.[35] When 1:100 dilutions of such reactions were probed with nanopores, three blockade types were observed (Figure 3B). Blockade B1 ($I_{res\%}$ = 73.9 ± 0.2%, N = 3, τ_{off} = 898 ± 198 ms) corresponds to the E2 alone, as it showed the same current blocked level observed for recombinant E2 (Figure S1B) and *in vitro* ubiquitination reactions lacking ATP (Figure 3A). Blockades B2 ($I_{res\%}$ = 64.0 ± 0.7%, N = 3, τ_{off} = 1602 ± 626 ms) and B3 ($I_{res\%}$ = 51.8 ± 0.8%, N = 3, τ_{off} = 1930 ± 764 ms) therefore represent ubiquitinated forms of the E2, with B2 likely corresponding to monoubiquitinated E2 (E2Ub) and B3, displaying a broader distribution of residual currents, corresponding to an E2 carrying two Ubs (E2Ub$_2$) (Figure 3B).

Our labeling of these latter two species, B2 and B3, rests on two observations: volume exclusion consideration suggests that deeper blockades (as determined by a lower $I_{res\%}$ value) should correspond to a larger protein inside ClyA; hence B3 should
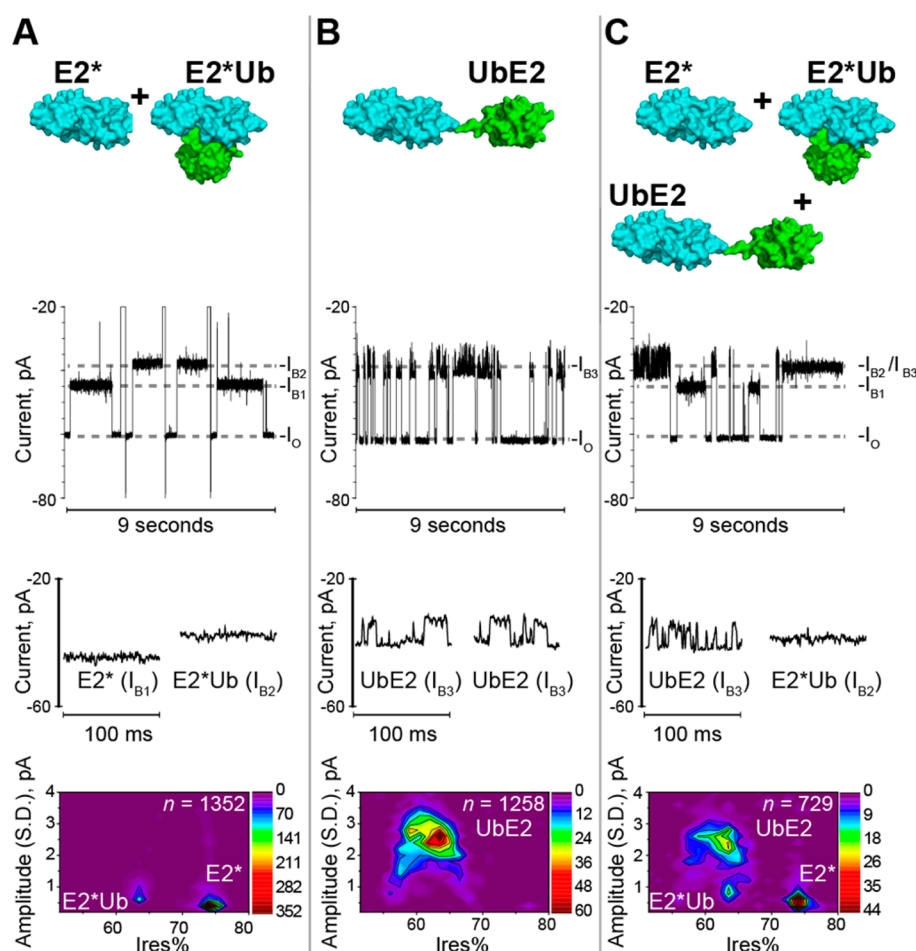
Figure 4. Discrimination of isomeric E2Ub conjugates. (A) From top to bottom: Surface representation of the E2 mutant (C116K, E2*) and E2* conjugated to Ub at its active site (E2*Ub, constructed with PyMOL) with below given a continuous representative trace of the *in vitro* ubiquitination reaction of E2* analyzed with ClyA nanopores (I_O = open pore, I_{B1} = blockade level elicited by E2, I_{B2} = E2*Ub); zoom-ins for blockades elicited by E2 and E2Ub; contour plot of all obtained blockades of an experiment. The same *in vitro* ubiquitination reaction was run on a Coomassie gel (lane 4, Figure S1A); a 1:50 dilution, or 120 nM E2*/E2*Ub, was used in experiments with the nanopore). (B) From top to bottom: Surface representation of N-terminally fused E2Ub protein (UbE2), constructed with PyMOL, and below a representative trace of 200 nM purified UbE2 analyzed with ClyA nanopores (I_{B3} = blockade level elicited by UbE2); zoom-ins provided for two blockades of UbE2; and blockades of an experiment depicted as a contour plot. (C) From top to bottom: Surface representation of E2*, E2*Ub, and UbE2; the proteins analyzed here in a mixture. Below are the same plots as in A and B shown but with 100 nM UbE2 and 1:50 dilution of an *in vitro* reaction (thus about 120 nM of E2* or E2*Ub) added to the *cis* side. Buffer used in all experiments: 150 mM NaCl, 50 mM TrisHCl, pH 7.5. Data were recorded using a 2 kHz low-pass Bessel filter with a 10 kHz sampling rate. All traces shown were postacquisition digitally filtered with a 500 Hz Gaussian low-pass filter.

represent a larger molecular weight species than B2. Second, ratios of the nanopore observed blockades (39 ± 2% B1, 46 ± 3% B2, 15 ± 1% B3) match reasonably well with data obtained from quantification of the Coomassie-stained SDS-PAGE gel (Figure 2) of the same *in vitro* reaction (47% E2, 47% E2Ub, 5% E2Ub$_2$). The differences between the two measurements might reflect different capture efficiencies between E2 and E2 conjugates and the semiquantitative nature of protein quantifications from Coomassie-stained gels. Thus, our data demonstrate that ClyA can directly discriminate between a protein and its mono- and poly-Ub conjugates.

ClyA Can Discriminate between Two Isomeric E2Ub Conjugates. We observed that the blockades of E2Ub (and E2Ub$_2$) of the *in vitro* reaction were wider in their distribution of residual current when compared to those of E2 alone (*i.e.*, the peak is wider, Figure 3B, histogram). We postulated that this may be due to the presence of isomeric forms of E2Ub. Isolation of the Coomassie-stained band from SDS-PAGE

corresponding to E2Ub, followed by mass spectrometry (Figure S3), identified three potential ubiquitination sites on the E2 (lysine residues 35, 39, and 121). These data confirmed the presence of at least three isomeric forms of E2Ub in our samples, although their relative concentration could not be assessed.

To investigate if nanopores can be used to discriminate between two isomeric E2Ub molecules, we sought to create well-defined E2Ub conjugates. This was achieved by exchanging the active site cysteine residue of the E2 for a lysine, creating E2-C116K (henceforth E2*). Such mutant E2s can accept Ub from the E1 on the active site (albeit at a reduced rate) but are unable to transfer the Ub further, creating a homogeneously ubiquitinated E2.[38] On a Coomassie-stained SDS-PAGE gel, we detected only a single major upper band (Figure S1A) corresponding to E2* monoubiquitinated on residue 116 (E2*Ub). Adding 10 μL of *in vitro* ubiquitination reaction of E2* to ClyA (1:50 dilution, Figure 4A) resulted in
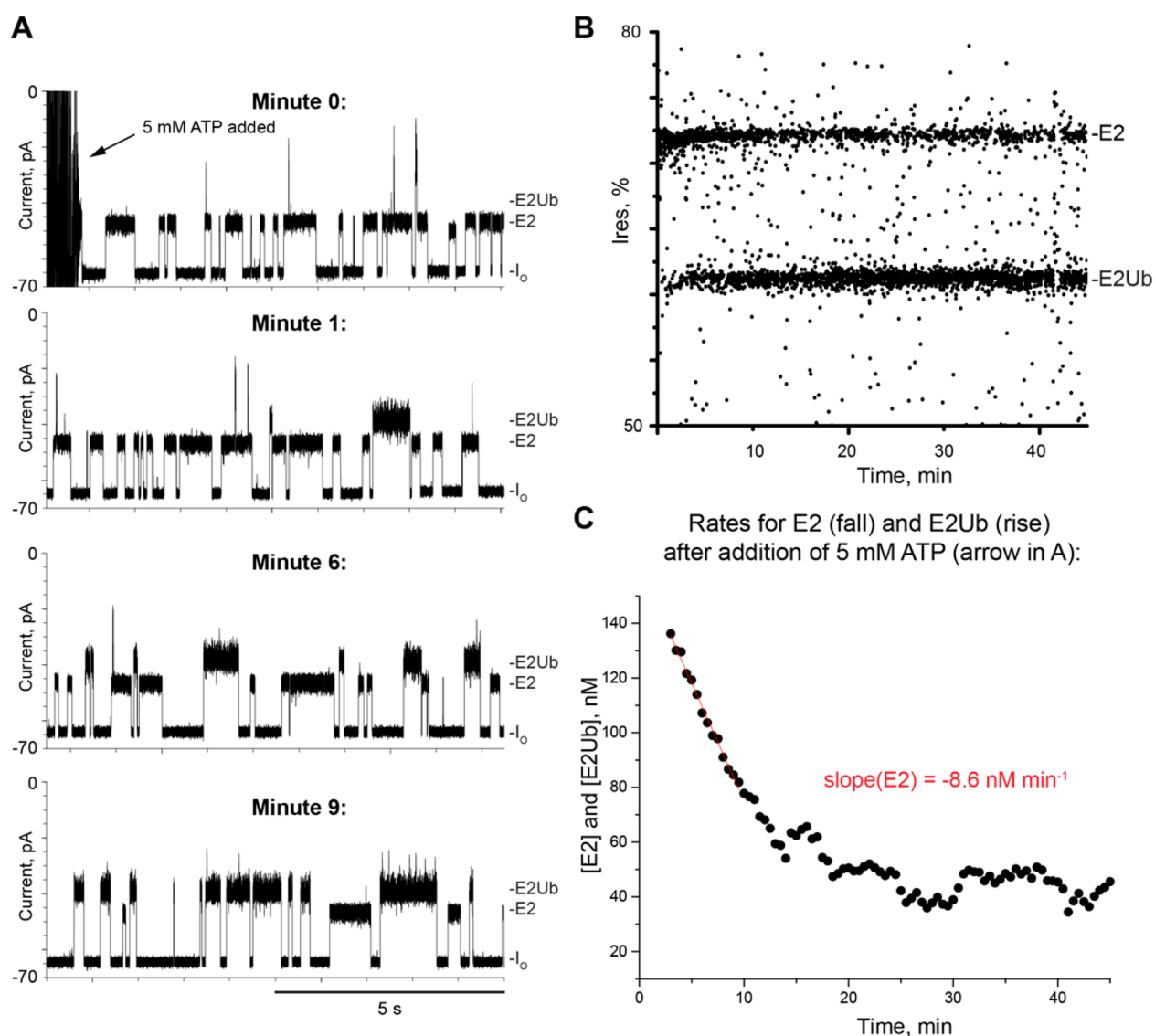
D

Figure 5. Real-time observation of protein-ubiquitination with the ClyA nanopore. (A) Representative traces from a real-time ubiquitination reaction further analyzed in (B) and (C). E1 (26.6 nM), E2 (160 nM), Ub (320 nM), and MgCl$_2$ (5 mM) are present in the *cis* buffer (150 mM NaCl, 50 mM TrisHCl, pH 7.5, ~23 °C). Blockades corresponding to E2Ub appear within 1 min and become the dominant type of events within 10 min. (B) All blockades individually represented as dots *versus* time. (C) Determination of the rate of E2 disappearance. The concentration of E2 was measured from the frequencies of current blockades as described in the Methods section. Linear fits (Origin, OriginLab, thin line) were used to determine the initial rate of the reaction. Data were collected at −35 mV using a 2 kHz low-pass Bessel filter with a 10 kHz sampling rate.

blockades corresponding to the unmodified E2 (B1, $I_{res\%}$ = 73.5 ± 0.1%, N = 3, τ_{off} = 503 ± 103 ms) as well as in 30% of the cases extra blockades that displayed $I_{res\%}$ values and dwell times ($I_{res\%}$ = 63.2 ± 0.1%, N = 3, τ_{off} = 2105 ± 600 ms) similar to those of E2Ub conjugates (Figure 3B). To create a second well-defined E2Ub conjugate, we fused Ub genetically to E2 at its N-terminus (UbE2) and expressed the construct recombinantly. E2*Ub and UbE2 were thus isomeric proteins, apart from the active site cysteine in UbE2 which is a lysine in E2*Ub. It should be noted that the exchange of cysteine for a lysine did not alter the blockades observed for E2* and E2 (Figures 3A and 4A). SDS-PAGE and Coomassie staining of E2*Ub and recombinantly purified UbE2 (Figure S4) demonstrated that both proteins ran almost identically on gel, making them virtually impossible to separate by this technique.

UbE2 (200 nM) showed blockades (Figure 4B) with, on average, similar residual currents as E2*Ub ($I_{res\%}$ = 62.5 ± 1.8%, N = 3, τ_{off} = 307 ± 126 ms, k_c = 16.7 ± 1.7 s^{-1} μM^{-1}) but wider in their distribution (Figure 4A). Further, the average dwell time was ~4-fold shorter than that for E2*Ub, enabling, partially, the discrimination of both isoforms by plotting the dwell time over the residual current (Figure S5). We also noticed that UbE2 blockades displayed a significantly higher SD of the current amplitude when compared to those caused by E2*Ub. The signals from the two isomeric species could be reliably separated by expressing the SD of the amplitude *versus* the residual current of the blockades caused by each species (Figure 4C, bottom). Taken together, our data demonstrate that ClyA can discriminate between isomeric E2Ub conjugates.

Real-Time Observation of Protein Ubiquitination under Physiological Conditions. Our data suggest that the

nanopore system can be employed to observe the kinetics of ubiquitination of E2 in real time. Using the same physiological buffer mixture as used for analyzing end-point reactions, we added 5 mM MgCl$_2$, 1 mM DTT, E1 (26.6 or 5.3 nM), Ub (320 nM), and E2 (160 nM) proteins to the *cis* side of ClyA. As expected, we observed only blockades corresponding to E2 from reactions performed without ATP. When we added 5 mM ATP to the same side, blockades corresponding to E2Ub appeared almost immediately, with the reaction reaching a plateau after 10−15 min (Figure 5 and Figure S6) when 26.6 nM E1 was present. The dwell time of E2 and E2Ub was shortened to 356 ± 154 and 528 ± 271 ms (N = 6, combined for reactions containing either 26.6 or 5.3 nM E1), respectively, most likely to the effect of MgCl$_2$ concentrations. The observed rate of the reaction could be obtained by following either the disappearance of E2 blockades or the appearance of E2Ub blockades (Figure 5B). We used the frequency of E2 blockades to measure the concentration of E2 in solution (Figure 5C and Figure S6; Methods). The slope of the linear regressions to the initial rates of E2 disappearance, −10.1 ± 3.9 nM min^{-1}, gave the rate of the loading of E1 with Ub under hydrolysis of ATP and the transfer of Ub to E2 from the E1 enzyme. As expected for an enzymatic reaction, decreasing E1 to 5.3 nM reduced the rate of the reaction accordingly to −1.1 ± 0.3 nM min^{-1} (Figure S6). In contrast to *in vitro* reaction experiments monitored by gel electrophoresis, even after 3 h, we only observed very few blockades which could be attributed to E2 carrying two ubiquitin molecules, an effect most likely due to the much reduced concentration of reactants used in the nanopore experiments. Taken together, our data show that nanopores can be employed to follow the ubiquitination cascade at the single-molecule level in real time.

CONCLUSION

The function of many proteins is regulated by ubiquitination: the covalent attachment of ubiquitin to substrate protein side chains. Since aberrant ubiquitination has been related to disease,[4] the detection of different ubiquitinated species in biological samples could help monitoring the onset of diseases. Commonly, gel electrophoresis is employed to detect and separate proteins in their mono- and polyubiquitinated forms, whereas mass spectrometry is the method of choice for detecting and characterizing ubiquitination *de novo*. Such techniques, however, are expensive and/or require lengthy preparation procedures. In this work, we showed that a biological nanopore can be employed to resolve protein and protein−ubiquitin adducts. Using defined monoubiquitin proteins, we could demonstrate that ClyA can resolve also isomeric ubiquitin-carrying proteins. Therefore, the ClyA nanopores could provide a low-cost method to monitor aberrant ubiquitination in a biological sample. However, similarly to all analytical techniques used in proteomics, the identification of proteins in complex biological samples will most likely require suppressing the signal from background proteins. This could be achieved, for example, using selective binding molecules to enrich target ubiquitinated proteins near the nanopore mouth,[13] while current recordings will be used to detect and quantify subpopulations of target proteins.

We also showed that the nanopore system is able to monitor the ubiquitination of native proteins in real time under physiological conditions. *In vitro* kinetic analysis of post-translational modifications is often challenging because the covalent modification of proteins is usually not associated with

a change in a spectroscopic signal. For example, ubiquitination may only be monitored in real time using the change in fluorescence polarization that follows the conjugation of a fluorescently labeled ubiquitin to its substrate.[39] Labeled ubiquitin, however, may alter affinity with substrate proteins while the fluorescent signal cannot distinguish between different ubiquitinated proteins, hence precluding monitoring intermediates and the E1−E2−E3 ubiquitination cascade. Crucially, because the signal allows recognition and discrimination of single proteins, the nanopore approach should allow following reaction intermediates and the simultaneous ubiquitination of different substrates. Thus, the nanopore approach could be expanded to follow, for example, the transfer of Ub from E2 to HECT domain E3s and even to substrates, following effectively the whole cascade concomitantly. This has potential applications when measuring the effect of small-molecule[40] and peptide[41] inhibitors or binding partners[35] of a certain component of the Ub cascade upon the whole ubiquitination cascade. Also, pathways that involve ubiquitin-like proteins such as SUMO, NEDD8, or ISG15[42] could be studied with the nanopore approach. Taken together, here we introduce a nanopore method that is immediately applicable to follow the ubiquitination of proteins of about 20−50 kDa in size. Solid-state or biological nanopores with wider diameters might be employed to monitor larger proteins.

METHODS

Plasmid Construction, Protein Expression, and Purification. In this work, we used an engineered variant of ClyA from *Salmonella typhi*, ClyA-AS (C87A/L99Q/E103G/F166Y/I203V/C285S/K294R/H307Y), as a template for the preparation of a ClyA variant containing a ring of tryptophan residues at position 56. The rationale behind this is that a ring of bulky, hydrophobic residues in the nanopore lumen might promote the target protein to dwell longer in the pore because of a smaller diameter of the pore and stronger interaction with the lumen.

The ClyA-AS-Q56W variant was prepared according to the MEGAWHOP procedure.[43] Part of the ClyA gene was amplified using the primer containing the Q56W substitution (forward, 5′-GAATACAGTT*GGG*AAGCGTCC-3′) and the T7 promotor (reverse, 5′-GCTAGTTATTGCTCAGCGG-3′). REDTaq ReadyMix (150 μL) was mixed with 6 μM of forward and reverse primers and ~400 ng of plasmid template, and PCR water was added to reach a final volume of 0.3 mL. After a preincubation step at 95 °C for 3 min, the reaction was cycled 27 times according to the cycling protocol: denaturation at 95 °C for 15 s, annealing at 55 °C for 15 s, extension at 72 °C for 2 min. The resulting PCR product was concentrated using the QIAquick PCR purification kit (Qiagen) and gel-purified using the QIAquick gel extraction kit. About 500 ng of the purified PCR product was mixed with ~300 ng of the ClyA-AS DNA template and the amplification was carried out with Phire Hot Start II DNA polymerase in 50 μL final volume. After 30 s preincubation at 98 °C, the reaction was cycled 30 times according to the following cycling protocol: denaturation at 98 °C for 5 s, extension at 72 °C for 1.5 min. The circular template was eliminated by incubation with Dpn I (1 FDU) for 1 h at 37 °C. Next, 0.6 μL of the resulting mixture was transformed into 50 μL of E. cloni 10G cells (Lucigen) by electroporation. The transformed bacteria were grown overnight at 37 °C on ampicillin (100 μg/mL) LB agar plates. The identity of the clones was confirmed by sequencing.

ClyA-AS and ClyA-AS-Q56W contain a C-terminal hexa-histidine tag. Monomers were expressed in E. cloni EXPRESS BL21 (DE3) cells (Lucigen) and purified using Ni-NTA affinity chromatography as described before.[37] Oligomers were then formed by adding 0.2% *n*-dodecyl-β-D-maltoside (DDM, GLYCON Biochemicals GmbH). Type I ClyA oligomers were separated from monomers and several other oligomeric ClyA forms[37] using a blue-native polyacrylamide gel

electrophoresis (BN-PAGE, Bio-Rad). In this work, we gel-extracted the lowest band, which is likely to correspond to the 12-meric (Type I) form of ClyA. Aliquots were stored at 4 °C in 150 mM NaCl, 15 mM Tris.HCl, pH 7.5 supplemented with 0.2% DDM and 10 mM EDTA.

The active site mutant form of Ubc4p (E2*) was constructed using the Quikchange site-directed mutagenesis kit (Stratagene), using the primer pair Ubc4 C-K F (5′-ATCAATGCCAATGGTAACAT-CAAACTGGACATCCTAAAGGATCAATG-3′) and Ubc4 C-K R (5′-CATTGATCCTTTAGGATGTCCAGTTTGATGTTAC-CATTGGCATTGAT-3′). The plasmid for expressing Ub fused to the N-terminus of Ubc4 (UbE2) was constructed as follows: UbE2 was synthesized as gBlock DNA fragment (Integrated DNA Technologies), digested with NcoI and BamHI, and cloned into NcoI-BamHI cut pET15b. Wild-type and mutant forms of Ubc4p were expressed and purified as described previously.[44] Human E1 (Ube1) was expressed and purified as described before.[45]

In Vitro **Ubiquitination Reactions.** *In vitro* ubiquitination reactions were performed essentially as described previously.[44] Reactions were performed in 25 mM TrisHCl, pH 8, 75 mM NaCl, 5 mM MgCl$_2$, containing 0.4 μM E1 (Ube1), 6 μM E2 (Ubc4), and 12 μM Ub (BostonBiochem) with or without 5 mM ATP. Reactions with wild-type E2 were incubated for 2.5 h at 35 °C with 800 rpm shaking, whereas reactions of the active site mutant form of the E2 (E2*) were incubated for 16 h at 35 °C with shaking. For SDS-PAGE and Coomassie staining, samples were quenched with SDS-PAGE buffer containing 5% β-mercaptoethanol and heated for 5 min at 95 °C prior to loading on a 15% SDS-PAGE gel.

Image Densitometry with ImageJ. For analysis of the Coomassie-stained gel, the ImageJ function "Plot Profile" was used. After subtraction of the image background (rolling ball radius, 50 pixels), a line was drawn across the bands of interest and the "Plot Profile" function used. The resulting values were used to create a histogram in Clampfit (Molecular Devices) where Gaussian functions were fitted and the area under the curve was used to determine the relative percentages of the peaks.

Electrophysiological Recordings and Data Analysis. An aperture of about 100 μm in diameter was created in a polytetrafluoro-ethylene film (Goodfellow Cambridge Limited) by applying a high-voltage spark. After application of a drop (~10 μL) of a 5% hexadecane/pentane solution to the aperture and a short waiting period, in order to allow pentane to evaporate, 500 μL of buffer in 150 mM NaCl, 50 mM TrisHCl, pH 7.5, was added to both sides of the film. A drop of about 10 μL of 10 mg/mL 1,2-diphytanoyl-*sn*-glycero-3-phosphocholine (DPhPC, Avanti Polar Lipids), dissolved in pentane, was then added on top of the buffer on both sides. After pipetting up and down, a folded bilayer formed spontaneously with a capacitance between 80 and 150 pF, depending on the electro-physiological chamber used. Normally, the capacitance varies only slightly for a given chamber. Experiments were performed at room temperature (~23 °C).

Electronic signals were amplified using an Axopatch 200B (Molecular Devices) with digitization performed with a Digidata 1440 (Axon Instruments). A low-pass 2 kHz Bessel filter was applied upon recording with 10 kHz sampling rate. Clampex and Clampfit (Molecular Devices) and Microsoft Excel were used for recording and data analysis, respectively. For residual current determination, the single-channel search function of Clampfit was employed. Contour plots were made with Origin (OriginLab).

Dwell times (τ_{off}) and interevent times were calculated by fitting exponential functions to cumulative distributions. Numbers are mean $\pm$ SD from at least three independent recordings.

For real-time measurements, E2 blockades were counted in 3 min intervals with 0.5 min overlaps. The concentration of E2 at any given time point was obtained by multiplying the fraction of E2 of the total number of blockades (#E2/(#E2 + #E2Ub)) by the initial concentration of E2 (160 nM). Origin (OriginLab) was used for linear fittings for initial rates.

Mass Spectrometric Analysis. The Coomassie-stained E2Ub band was excised from gel and submitted for MS analysis. The gel fragment was washed with 100 mM ammonium bicarbonate and acetonitrile, resuspended in 100 mM ammonium bicarbonate, and proteolytic treatment was performed using trypsin. Peptides were extracted with 75% acetonitrile and 25% H$_2$O (5% formic acid in water) and analyzed by nanoliquid chromatography/tandem mass spectrometry (nLC-MS/MS).[46] MS data were analyzed with PEAKS 7.0 software (Bioinformatics Solutions Inc.).

ASSOCIATED CONTENT

Ⓢ Supporting Information

The Supporting Information is available free of charge on the ACS Publications website at DOI: 10.1021/acsnano.6b07760.

Information on protein sequences, additional electro-physiological recordings, Coomassie-stained gels on isomeric E2Ub conjugates, and results of mass spectrometry analysis, more data of real-time experiments as well as cumulative distributions for τ_{off} and τ_{on} measurements (PDF)

AUTHOR INFORMATION

Corresponding Authors
*E-mail: c.p.williams@rug.nl.
*E-mail: g.maglia@rug.nl.

ORCID Ⓘ
Carsten Wloka: 0000-0003-0487-3311

Notes
The authors declare no competing financial interest.

REFERENCES

(1) Hershko, A.; Heller, H.; Elias, S.; Ciechanover, A. Components of Ubiquitin-Protein Ligase System. Resolution, Affinity Purification, and Role in Protein Breakdown. *J. Biol. Chem.* **1983**, *258*, 8206−8214.

(2) Komander, D.; Rape, M. The Ubiquitin Code. *Annu. Rev. Biochem.* **2012**, *81*, 203−229.

(3) Kandimalla, R. J.; Anand, R.; Veeramanikandan, R.; Wani, W. Y.; Prabhakar, S.; Grover, V. K.; Bharadwaj, N.; Jain, K.; Gill, K. D. CSF Ubiquitin as a Specific Biomarker in Alzheimer's Disease. *Curr. Alzheimer Res.* **2014**, *11*, 340−348.

(4) Popovic, D.; Vucic, D.; Dikic, I. Ubiquitination in Disease Pathogenesis and Treatment. *Nat. Med.* **2014**, *20*, 1242−1253.

(5) Meier, F.; Abeywardana, T.; Dhall, A.; Marotta, N. P.; Varkey, J.; Langen, R.; Chatterjee, C.; Pratt, M. R. Semisynthetic, Site-Specific Ubiquitin Modification of Alpha-Synuclein Reveals Differential Effects on Aggregation. *J. Am. Chem. Soc.* **2012**, *134*, 5468−5471.

(6) Jin, H.; Zangar, R. C. Protein Modifications as Potential Biomarkers in Breast Cancer. *Biomark Insights* **2009**, *4*, 191−200.

(7) Schmid, A. W.; Fauvet, B.; Moniatte, M.; Lashuel, H. A. Alpha-Synuclein Post-Translational Modifications as Potential Biomarkers for Parkinson Disease and Other Synucleinopathies. *Mol. Cell. Proteomics* **2013**, *12*, 3543−3558.

(8) Madiraju, C.; Welsh, K.; Cuddy, M. P.; Godoi, P. H.; Pass, I.; Ngo, T.; Vasile, S.; Sergienko, E. A.; Diaz, P.; Matsuzawa, S.; Reed, J. C. TR-FRET-Based High-Throughput Screening Assay for Identification of Ubc13 Inhibitors. *J. Biomol. Screening* **2012**, *17*, 163–176.

(9) Mot, A. C.; Prell, E.; Klecker, M.; Naumann, C.; Faden, F.; Westermann, B.; Dissmeyer, N. Real-Time Detection of PRT1-Mediated Ubiquitination Via Fluorescently Labeled Substrate Probes. *New Phytol.* **2017**, DOI: 10.1111/nph.14497.

(10) Toseland, C. P. Fluorescent Labeling and Modification of Proteins. *J. Chem. Biol.* **2013**, *6*, 85–95.

(11) Gu, L. Q.; Braha, O.; Conlan, S.; Cheley, S.; Bayley, H. Stochastic Sensing of Organic Analytes by a Pore-Forming Protein Containing a Molecular Adapter. *Nature* **1999**, *398*, 686–690.

(12) Guan, X.; Gu, L. Q.; Cheley, S.; Braha, O.; Bayley, H. Stochastic Sensing of TNT with a Genetically Engineered Pore. *ChemBioChem* **2005**, *6*, 1875–1881.

(13) Soskine, M.; Biesemans, A.; Moeyaert, B.; Cheley, S.; Bayley, H.; Maglia, G. An Engineered ClyA Nanopore Detects Folded Target Proteins by Selective External Association and Pore Entry. *Nano Lett.* **2012**, *12*, 4895–4900.

(14) Fahie, M. A.; Yang, B.; Mullis, M.; Holden, M. A.; Chen, M. Selective Detection of Protein Homologues in Serum Using an OmpG Nanopore. *Anal. Chem.* **2015**, *87*, 11143–11149.

(15) Luchian, T.; Shin, S. H.; Bayley, H. Kinetics of a Three-Step Reaction Observed at the Single-Molecule Level. *Angew. Chem., Int. Ed.* **2003**, *42*, 1926–1929.

(16) Luchian, T.; Shin, S. H.; Bayley, H. Single-Molecule Covalent Chemistry with Spatially Separated Reactants. *Angew. Chem., Int. Ed.* **2003**, *42*, 3766–3771.

(17) Ho, C. W.; Van Meervelt, V.; Tsai, K. C.; De Temmerman, P. J.; Mast, J.; Maglia, G. Engineering a Nanopore with Co-Chaperonin Function. *Sci. Adv.* **2015**, *1*, e1500905.

(18) Lee, J.; Boersma, A. J.; Boudreau, M. A.; Cheley, S.; Daltrop, O.; Li, J.; Tamagaki, H.; Bayley, H. Semisynthetic Nanoreactor for Reversible Single-Molecule Covalent Chemistry. *ACS Nano* **2016**, *10*, 8843–8850.

(19) Kasianowicz, J. J.; Brandin, E.; Branton, D.; Deamer, D. W. Characterization of Individual Polynucleotide Molecules Using a Membrane Channel. *Proc. Natl. Acad. Sci. U. S. A.* **1996**, *93*, 13770–13773.

(20) Wescoe, Z. L.; Schreiber, J.; Akeson, M. Nanopores Discriminate among Five C5-Cytosine Variants in DNA. *J. Am. Chem. Soc.* **2014**, *136*, 16582–16587.

(21) An, N.; Fleming, A. M.; Burrows, C. J. Human Telomere G-Quadruplexes with Five Repeats Accommodate 8-Oxo-7,8-Dihydroguanine by Looping out the DNA Damage. *ACS Chem. Biol.* **2016**, *11*, 500–507.

(22) Johnson, R. P.; Fleming, A. M.; Beuth, L. R.; Burrows, C. J.; White, H. S. Base Flipping within the Alpha-Hemolysin Latch Allows Single-Molecule Identification of Mismatches in DNA. *J. Am. Chem. Soc.* **2016**, *138*, 594–603.

(23) Siwy, Z.; Trofin, L.; Kohli, P.; Baker, L. A.; Trautmann, C.; Martin, C. R. Protein Biosensors Based on Biofunctionalized Conical Gold Nanotubes. *J. Am. Chem. Soc.* **2005**, *127*, 5000–5001.

(24) Han, A. P.; Schurmann, G.; Mondin, G.; Bitterli, R. A.; Hegelbach, N. G.; de Rooij, N. F.; Staufer, U. Sensing Protein Molecules Using Nanofabricated Pores. *Appl. Phys. Lett.* **2006**, *88*, 093901.

(25) Oukhaled, A.; Bacri, L.; Pastoriza-Gallego, M.; Betton, J. M.; Pelta, J. Sensing Proteins through Nanopores: Fundamental to Applications. *ACS Chem. Biol.* **2012**, *7*, 1935–1949.

(26) Mohammad, M. M.; Movileanu, L. Protein Sensing with Engineered Protein Nanopores. *Methods Mol. Biol. (N. Y., NY, U. S.)* **2012**, *870*, 21–37.

(27) Nivala, J.; Mulroney, L.; Li, G.; Schreiber, J.; Akeson, M. Discrimination among Protein Variants Using an Unfoldase-Coupled Nanopore. *ACS Nano* **2014**, *8*, 12365–12375.

(28) Pastoriza-Gallego, M.; Rabah, L.; Gibrat, G.; Thiebot, B.; van der Goot, F. G.; Auvray, L.; Betton, J. M.; Pelta, J. Dynamics of Unfolded Protein Transport through an Aerolysin Pore. *J. Am. Chem. Soc.* **2011**, *133*, 2923–2931.

(29) Nivala, J.; Marks, D. B.; Akeson, M. Unfoldase-Mediated Protein Translocation through an Alpha-Hemolysin Nanopore. *Nat. Biotechnol.* **2013**, *31*, 247–250.

(30) Rodriguez-Larrea, D.; Bayley, H. Multistep Protein Unfolding During Nanopore Translocation. *Nat. Nanotechnol.* **2013**, *8*, 288–295.

(31) Pastoriza-Gallego, M.; Breton, M. F.; Discala, F.; Auvray, L.; Betton, J. M.; Pelta, J. Evidence of Unfolded Protein Translocation through a Protein Nanopore. *ACS Nano* **2014**, *8*, 11350–11360.

(32) Cressiot, B.; Braselmann, E.; Oukhaled, A.; Elcock, A. H.; Pelta, J.; Clark, P. L. Dynamics and Energy Contributions for Transport of Unfolded Pertactin through a Protein Nanopore. *ACS Nano* **2015**, *9*, 9050–9061.

(33) Rosen, C. B.; Rodriguez-Larrea, D.; Bayley, H. Single-Molecule Site-Specific Detection of Protein Phosphorylation with a Nanopore. *Nat. Biotechnol.* **2014**, *32*, 179–181.

(34) Nir, I.; Huttner, D.; Meller, A. Direct Sensing and Discrimination among Ubiquitin and Ubiquitin Chains Using Solid-State Nanopores. *Biophys. J.* **2015**, *108*, 2340–2349.

(35) Williams, C.; van den Berg, M.; Panjikar, S.; Stanley, W. A.; Distel, B.; Wilmanns, M. Insights into Ubiquitin-Conjugating Enzyme/Co-Activator Interactions from the Structure of the Pex4p:Pex22p Complex. *EMBO J.* **2012**, *31*, 391–402.

(36) Banka, P. A.; Behera, A. P.; Sarkar, S.; Datta, A. B. Ring E3-Catalyzed E2 Self-Ubiquitination Attenuates the Activity of Ube2E Ubiquitin-Conjugating Enzymes. *J. Mol. Biol.* **2015**, *427*, 2290–2304.

(37) Soskine, M.; Biesemans, A.; De Maeyer, M.; Maglia, G. Tuning the Size and Properties of ClyA Nanopores Assisted by Directed Evolution. *J. Am. Chem. Soc.* **2013**, *135*, 13456–13463.

(38) Plechanovova, A.; Jaffray, E. G.; Tatham, M. H.; Naismith, J. H.; Hay, R. T. Structure of a Ring E3 Ligase and Ubiquitin-Loaded E2 Primed for Catalysis. *Nature* **2012**, *489*, 115–120.

(39) Worden, E. J.; Padovani, C.; Martin, A. Structure of the Rpn11-Rpn8 Dimer Reveals Mechanisms of Substrate Deubiquitination During Proteasomal Degradation. *Nat. Struct. Mol. Biol.* **2014**, *21*, 220–227.

(40) Ceccarelli, D. F.; Tang, X.; Pelletier, B.; Orlicky, S.; Xie, W.; Plantevin, V.; Neculai, D.; Chou, Y. C.; Ogunjimi, A.; Al-Hakim, A.; Varelas, X.; Koszela, J.; Wasney, G. A.; Vedadi, M.; Dhe-Paganon, S.; Cox, S.; Xu, S.; Lopez-Girona, A.; Mercurio, F.; Wrana, J.; Durocher, D.; Meloche, S.; Webb, D. R.; Tyers, M.; Sicheri, F. An Allosteric Inhibitor of the Human Cdc34 Ubiquitin-Conjugating Enzyme. *Cell* **2011**, *145*, 1075–1087.

(41) Zhao, B.; Choi, C. H.; Bhuripanyo, K.; Villhauer, E. B.; Zhang, K.; Schindelin, H.; Yin, J. Inhibiting the Protein Ubiquitination Cascade by Ubiquitin-Mimicking Short Peptides. *Org. Lett.* **2012**, *14*, 5760–5763.

(42) Herrmann, J.; Lerman, L. O.; Lerman, A. Ubiquitin and Ubiquitin-Like Proteins in Protein Regulation. *Circ. Res.* **2007**, *100*, 1276–1291.

(43) Miyazaki, K. Megawhop Cloning: A Method of Creating Random Mutagenesis Libraries Via Megaprimer PCR of Whole Plasmids. *Methods Enzymol.* **2011**, *498*, 399–406.

(44) Williams, C.; van den Berg, M.; Geers, E.; Distel, B. Pex10p Functions as an E3 Ligase for the Ubc4p-Dependent Ubiquitination of Pex5p. *Biochem. Biophys. Res. Commun.* **2008**, *374*, 620–624.

(45) Chou, Y. C.; Keszei, A. F.; Rohde, J. R.; Tyers, M.; Sicheri, F. Conserved Structural Mechanisms for Autoinhibition in IpaH Ubiquitin Ligases. *J. Biol. Chem.* **2012**, *287*, 268–275.

(46) Dashty, M.; Motazacker, M. M.; Levels, J.; de Vries, M.; Mahmoudi, M.; Peppelenbosch, M. P.; Rezaee, F. Proteome of Human Plasma Very Low-Density Lipoprotein and Low-Density Lipoprotein Exhibits a Link with Coagulation and Lipid Metabolism. *Thromb. Haemostasis* **2014**, *111*, 518–530.

(47) Mueller, M.; Grauschopf, U.; Maier, T.; Glockshuber, R.; Ban, N. The Structure of a Cytolytic Alpha-Helical Toxin Pore Reveals Its Assembly Mechanism. *Nature* **2009**, *459*, 726–730.